Battery Charging Considerations in Small Scale Electricity Generation from a Thermoelectric Module

C. E. Kinsella[1], S. M. O'Shaughnessy[1], M.J. Deasy[1], M. Duffy[2], A.J. Robinson[1]*

[1]Department of Mechanical & Manufacturing Engineering, Parsons Building, Trinity College Dublin, Ireland.
[2] Electrical and Electronic Engineering, NUI Galway, Ireland
**Email: arobins@tcd.ie*
**Tel: +353 1 896 3919*

Abstract
This project involves the development of a prototype electrical generator for delivering and storing small amounts of electricity. Power is generated using the thermoelectric effect. A single thermoelectric generator (TEG) is utilised to convert a small portion of the heat flowing through it to electricity. The electricity produced is used to charge a single rechargeable 3.3 Volt lithium-iron phosphate battery. This study investigates methods of delivering maximum power to the battery for a range of temperature gradients across the thermoelectric module. The paper explores load matching and maximum power point tracking techniques. It was found that, for the TEG tested, a SEPIC DC-DC converter was only beneficial for temperature gradients less than 100 ºC across the TEG. At a temperature gradient of 150 ºC, the effective resistance of the battery was close to the internal resistance of the TEG. For temperature gradients in excess of 100°C a DC-DC converter is not suggested and a simple charge protection circuit is sufficient.

Keywords
Thermoelectricity, Electricity Generation, Load Matching, Maximum Power Point Tracking

1. Introduction

Thermoelectric generators (TEGs) are solid state devices that convert heat directly to electricity. Although TEGs are commercially available, they are low in efficiency, typically of the order of 3-5%. This being the case, they are generally used in niche applications that require power in the range of 1 µW to 100 W [1].

The low efficiency of TEGs is compounded by the fact that for a given temperature differential the power generated by a TEG generator system is a function of the load resistance. Since there is a peak maximum power at a critical load resistance, the real life efficiency could be much less than the maximum possible efficiency if the load resistance is greater or less than this critical value. This is the case for both single TEG technologies, such as that reported in O'Shaughnessy et al. [2] as well as generators with multiple TEGs, such as that reported by Lesage and Page-Potvin [3]. Thus, a complete TEG generator design requires that not only the heat source, the TEG and the heat sink be modelled, but also the effective impedance of the electrical load to which the TEG is supplying electricity.

Recent work with regard to testing and modelling thermoelectric modules aims to provide the theoretical framework to predict the electrical output characteristics given the thermal boundary conditions on the hot and cold faces of the TEG. Based on the works of Sandoz-Rosadoi and Stevens [4], Rodrigez et al. [5], Hodes [6] and Hsu et al. [7], it can be said that theoretical modelling of thermoelectric generators is mature. On the other hand, there has been less attention paid to technologies which ensure that the maximum power is being drawn from the TEG for the given thermal loading condition.

Eakburanawat and Boonyaroonate [8] developed a SEPIC DC-DC converter that was controlled by a microcontroller to optimally charge a battery from thermoelectric modules. Maximum power was transferred to the battery when the input impedance of the DC-DC converter matched the impedance of the battery. The input impedance of the DC-DC converter was changed by varying the duty cycle of the pulse width modulated (PWM) signal applied to the gate of the MOSFET. Six Taihuaxing TEGs (TEP-1264-1.5) were connected in series to give a combined internal resistance of 17.8 Ω at 140 °C. These were then used to charge a 6 V battery with internal resistance of 0.1 Ω. Three experiments were set up: in the first experiment, the TEGs were directly connected to the battery. The maximum power transferred to the battery was 6.35 W. In the second experiment, a SEPIC converter was introduced with the duty cycle fixed at 35%. In this case the power transferred to the battery was 7.63 W. In the third experiment, the duty cycle of the MOSFET was varied throughout the experiment in order to deliver maximum power to the battery. This was implemented by measuring the current into the battery and varying the duty cycle until maximum current flowed into the battery. The Perturb and Observe maximum power point tracking (MPPT) technique was used, however only the current was measured as it was assumed that the battery voltage remained relatively constant. In this scenario 7.99 W was transferred to the battery and the SEPIC was found to be 95.11% efficient. The maximum power point tracking circuit was determined to be 15% more efficient than direct charging. It was also observed that during direct charging, if there was no temperature difference across the TEG, the TEG acted as a load and discharged the battery. This did not happen when the SEPIC was inserted.

In 2006, Nagayoshi [9] developed a buck-boost based maximum power point tracker to reduce the impedance mismatch between an array of thermoelectric modules and the load. The resistance of the load was varied from 3 Ω to 40 Ω. The

MPPT algorithm operated by increasing the duty cycle until the conductance of the load matched the internal conductance of the TEG array. If the effective conductance of the load was lower than that of the TEG array, boost mode was employed. Conversely, if the effective conductance of the load was higher than the internal conductance of the TEGs, buck mode was employed. The circuit was 80% efficient.

Nagayoshi et al. [10] later compared the output power with and without the maximum power point trackers. Two experimental rigs were set up. The first rig consisted of four strings of TEGs held at different temperature gradients: 40 °C, 70 °C, 100 °C and 130 °C. Within each string, the temperature was held constant. In the second rig, maximum power point trackers were placed on each string of TEGs. Nagayoshi et al. [10] compared the output power of each system with a range of load resistances. When a load of 5 Ω was applied, direct charging delivered more power than the MPPT method for the string of TEGs held at 70 °C and 100 °C. This highlights that while the internal resistance of the TEGs is temperature dependent, the resistance changes only slightly with temperature and thus if the load is matched at a given temperature, direct charging can be optimal even if this temperature fluctuates within a certain range.

Chen et al. [11] investigated power conditioning for thermoelectric modules. Ten TEGs were connected in series and a 40 Ω load was attached, which was close to the total internal resistance of the TEGs. At a temperature gradient of 119 °C, the output power of the TEGs was calculated to be 50.6 W. The 40 Ω load was then replaced by a light bulb and the TEG output power dropped to 23 W. A maximum power point tracker was then developed using a boost DC-DC converter with synchronous rectification and the Perturb & Observe method. Efficiencies of 95.3% were achieved. The maximum power transferred to the light bulb was 47 W. This increase in power was due to load matching.

Vieira et al. [12] designed and built a maximum power point tracker to optimally charge a lead acid battery using a thermoelectric module. The MPPT was based on a SEPIC circuit working in continuous conduction mode and the Perturb and Observe method was employed to find the maximum power point. In the algorithm, charge protection was also implemented to protect the lead acid battery from over-charging. The experimental results showed that if the 12 V battery was directly connected to the TEG, the TEG generated 19 W, whereas if the MPPT was inserted between the TEG and the battery, the TEG produced 28.5W. The MPPT circuit produced 33% more power from the TEG than direct charging.

This paper focuses on charging a rechargeable battery using only one thermoelectric generator. The context of the research is for developing world applications, such as that reported by O'Shaughnessy et al. [2], where small amounts of electricity can be used to charge LED lanterns and low power demand mobile phones. Within this context, the specific objectives of this study are to:

- Select a thermoelectric module and fully characterise it at different temperature gradients and with different load resistances
- Select a battery and consider different methods of charging the battery
- Investigate DC-DC converters and MPPT algorithms
- Design a simple, easy to use battery charging circuit with the thermoelectric module as the power source

2. Overview of thermoelectricity

Thermoelectric generators are solid state energy devices which convert heat directly into electricity by means of the thermoelectric effect. TEGs have no moving parts and are commercially available in a variety of shapes, sizes and power ratings.

The working principle is depicted in Figure 1. A thermoelectric module is sandwiched between a heat source and a heat sink. Heat flows from the heat source across the module and is dissipated by the heat sink, and electricity is produced by the module. The thermoelectric module consists of pairs of p-n thermoelements. The positive (p-type) and negative (n-type) doped semiconductor elements are connected electrically in series and thermally in parallel. Initially, the conductors in the module possess a uniform distribution of charge carriers. However, the heat input to the module, Q_H, creates a temperature difference across the p-n thermoelements. The Seebeck effect is described by Rowe [13]. The free carriers at the hot end have greater kinetic energy and diffuse to the cold end. The accumulation of charge results in a back emf which resists further flow of charge. If the temperature difference across these junctions is maintained, an open circuit voltage V_{OC} is generated according to

$$V_{oc} = \alpha(T_h - T_c) \quad (1)$$

where α is the Seebeck coefficient and T_h and T_c are the 'hot' and 'cold' junction temperatures. The Seebeck coefficient is a thermoelectric material property. Rowe [14] describes the strength of thermoelectric materials, expressed by a quantity Z, known as the figure of merit. Z depends on the thermal and electrical properties of the material and on the Seebeck coefficient, α.

$$Z = \frac{\alpha^2 \sigma}{\lambda} = \frac{\alpha^2}{\rho \lambda} \tag{2}$$

where λ is the thermal conductivity, σ is the electrical conductivity, and ρ is the electrical resistivity. The majority of thermoelectric generators in current use are based on bismuth-telluride (Bi_2Te_3), lead-telluride (PbTe) or silicon-germanium (SiGe) alloy technologies. According to Rowe [14], Bi_2Te_3 generators have the greatest figure of merit, but are typically limited in their maximum operating temperature to approximately 250°C ~300°C. PbTe and SiGe generators have lower figures of merit but compensate with the ability to operate at much higher temperatures (~600°C for PbTe and ~1000°C for SiGe).

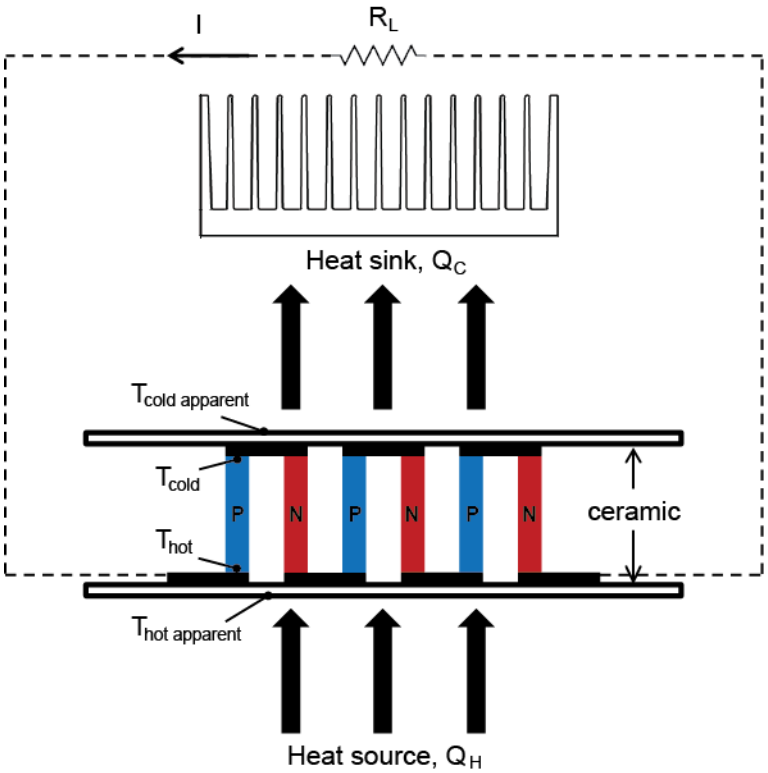

Figure 1: Thermoelectric power generation

A single thermocouple is depicted in Figure 2. The electrical resistance R and thermal conductance K of a thermocouple of length L and cross-sectional area A_p are defined respectively as [6]:

$$R_{TEG} = \frac{2\rho L}{A_p} \tag{3}$$

$$\mathrm{K} = \frac{2\lambda A_p}{L} \tag{4}$$

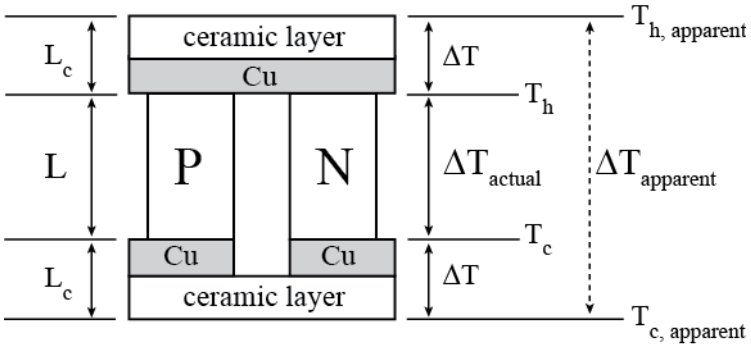

Figure 2: Diagram of a single thermoelectric thermocouple

By assuming one-dimensional conduction through the module, the rate of heat supply, Q_H, and heat removal, Q_C, can be estimated at the hot and cold junctions as [6]

$$Q_H = \mathrm{K}(\Delta T) + (\alpha_{p,n}) I T_h - \frac{I^2 R_{TEG}}{2} \tag{5}$$

$$Q_C = \mathrm{K}(\Delta T) + (\alpha_{p,n}) I T_c + \frac{I^2 R_{TEG}}{2} \tag{6}$$

where $\alpha_{p,n}$ is equal to $(\alpha_p - \alpha_n)$, and I is the current through the thermocouple. The electrical power generated by the TEG is given by the voltage and current across the external load, R_L. By applying an energy balance across the module, the electrical power, P_{elec}, is equal to the difference between heat delivered and dissipated, or $(Q_H - Q_C)$.

$$P_{elec} = Q_H - Q_C = \alpha_{pn} I \Delta \mathrm{T} - I^2 R_{TEG} \tag{7}$$

Equation 7 can be rearranged and simplified to give the voltage:

$$\mathrm{V} = \alpha_{pn} \Delta \mathrm{T} - \mathrm{I} R_{TEG} \tag{8}$$

Equation 8 expresses the voltage as a function of current for a given temperature difference. Using the standard model [6] the parameter α_{pn} is measured by open-circuiting ($I = 0$) the TEG, and measuring the applied temperature difference and corresponding voltage. By setting P_{elec} equal to $I^2 R_L$ in Equation 7, where R_L is the load resistance, the current can be found from

$$\mathrm{I} = \frac{\alpha_{pn} \Delta T}{(R_L + R_{TEG})} \tag{9}$$

Substituting Equation 9 into Equation 7 yields an expression for the electrical power:

$$P_{elec} = (\alpha_{pn} \Delta T)^2 \frac{R_L}{(R_L + R_{TEG})^2} \tag{10}$$

A thermoelectric module generates maximum power when the module resistance matches the load resistance, i.e. when $R_L = R_{TEG}$ [15]. It follows that maximum power, P_{max}, is given by

$$P_{max} = \frac{(\alpha_{pn} \Delta T)^2}{4 R_{TEG}} = \frac{A_p (\alpha_{pn} \Delta T)^2}{8 \rho L} \tag{11}$$

From Equations 10 and 11, the power produced by each thermocouple is approximately proportional to its cross-sectional area, and inversely proportional to its length. Therefore, power produced by an entire module is dependent on the number of couples, N, as well as the ratio of the load resistance to that of the TEG itself. It should also be kept in mind that the internal resistance R_{TEG} of a thermoelectric module varies with temperature due to a variation in resistivity. The above theoretical framework was compared with experimental measurements in O'Shaughnessy et al. [2] and the agreement was adequate.

The equivalent circuit for a thermoelectric module can be represented by a voltage source, $\mathrm{V_{OC}}$, with a variable resistor in series, $\mathrm{R_{TEG}}$, as shown in Figure 3.

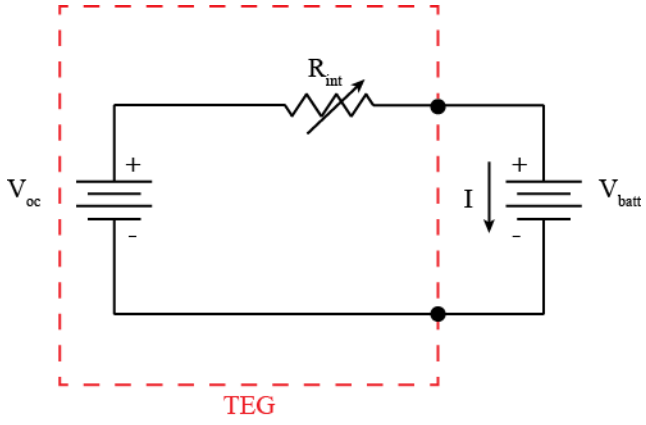

Figure 3: Equivalent circuit of a thermoelectric module connected to a load

For this study, a rechargeable battery is to be charged using the TEG as the power source. Therefore, to obtain maximum power from the TEG, the effective resistance of the battery must be comparable to the internal resistance of the TEG. Two approaches were investigated in this study:

- Select a battery with the same effective resistance as the internal resistance of the TEG
- Design a DC-DC converter to change the impedance of the load and then implement a MPPT device to continuously track the maximum power point

The disadvantage of the first approach is that the internal resistance of the TEG changes with temperature whilst the effective resistance of the battery changes with charging current. The disadvantage of the second approach is the increased complexity and the fact that electrical energy is required to operate the circuitry.

3. Thermoelectric module selection

The thermoelectric module chosen for this investigation was the TEG 12610-5.1 supplied by Thermal Electronics Corp, Canada. The output power from the thermoelectric modules was close to the specifications quoted by the manufacturer and could withstand temperatures of up to 320 °C intermittently.

The 40mm x40 mm TEG is composed of 126 Bismuth Telluride p-n junctions. While TEGs with larger area specify higher output power per degree temperature difference, a greater heat flux is required to maintain the same ΔT_{TEG}. According to the manufacturer's specification at ΔT_{TEG} = 210 °C, TEG1-12610-5.1 is capable of producing 5.9 W of electrical power at matched load. Some specifications for the module are provided in Table 1.

4. Battery selection

A variety of battery typologies were explored. Nickel metal hydride batteries are widely used due to their availability, low cost and low nominal voltage. However, nickel metal hydride batteries release hydrogen when they are over-charged, which can be hazardous. Lead acid batteries were also investigated. Although robust, lead acid batteries have low energy densities, making them significantly larger and heavier than other batteries of the same capacity.

Lithium ion batteries were then analysed. It was discovered experimentally that in some cases when they are overcharged the cell can rupture, leading to combustion. From further investigations into different types of lithium ion batteries, it was found that lithium iron phosphate batteries are inherently much safer than conventional lithium ion cells due to their olivine structure which changes only slightly when over-charged. Upon heating, no oxygen is evolved and there is no thermal runaway under abusive conditions [16]. They also possess high energy densities and long life cycles. The batteries exhibit very flat open circuit voltage curves over the State-of-Charge of the battery, which means the voltage of the battery stays relatively constant during discharge. They can also be left in a partially discharged state for extended periods without causing permanent damage. Lithium iron phosphate ($LiFePo_4$) batteries have been selected for this study, specifically the ANR26650 lithium-iron-phosphate cylindrical cell manufactured by A123 Systems. The battery was sourced from Korea and cost $11.30 per cell. Some battery specifications are provided in Table 2.

Table 1: TEG1-12610-5.1 supplier specifications

Dimensions	40 mm x 40 mm
Hot side temperature	260 °C
Cold side temperature	50 °C
Open circuit voltage	8.6 Volts
Internal resistance	3 Ohm
Match load output voltage	4.2 Volts
Match load output current	1.4Amps
Match load output power	5.9 Watts
Heat flow through the module	~ 140 Watts
Heat flux	~ 8.8 Watts/cm^2

Table 2: $LiFePo_4$ battery specifications

Cell dimensions (mm)	φ 26 x 65
Cell weight (g)	72
Cell capacity, nominal/minimum (Ah)	2.3/2.2
Voltage, nominal (V)	3.3
Internal impedance (mΩ)	8
Max. continuous discharge (A)	70
Operating temperature (°C)	-30 ~ 55
Typical cycle life	

>1,000

An advantage of $LiFePo_4$ batteries is their moderate operating voltage (typically 3.3 V) which is close to the matched load voltage of the thermoelectric module (4.2 V) at ΔT_{TEG} = 210 ℃. As the open circuit voltage of a thermoelectric module is directly proportional to the temperature difference across it, this suggests that at a $\Delta T_{TEG} \approx$ 150-160 ℃, the nominal voltage of the battery would be comparable to the matched load voltage of the TEG. The specifications suggest the maximum capacity of the battery is 7.59 Wh.

5. DC-DC Converters and Maximum Power Point Tracking

In order to investigate whether power transfer between the TEG and load could be improved, several DC-DC converters were initially investigated to provide a match between the impedance of the load to that of the TEG as it varied under differing thermal loads. Design parameters assumed for the different DC-DC converters are listed in Table 3.

Table 3: DC-DC converter specifications

Input TEG voltage	2 – 10 V
Output (battery) voltage (nominal)	3.3 V
Maximum output power	5.9 W

A boost converter, a non-inverting buck-boost converter and a SEPIC circuit were designed and constructed. The SEPIC circuit was ultimately chosen for the following reasons:

- Its ability to step up or step down the voltage as the open circuit voltage of the TEG was expected to vary between 0 ~ 10 V
- It demonstrated high efficiency
- It was possible to measure the open circuit voltage without an additional switch unlike the boost converter

The characteristic equation of a SEPIC is provided by Equation 12, where D is the duty cycle, V_{in} is the voltage at the input of the SEPIC and V_{out} is the voltage at the output of the SEPIC.

$$\frac{V_{out}}{V_{in}} = \frac{D}{1 - D} \tag{12}$$

Ignoring losses, Equation 13 demonstrates the relationship between the effective load resistance $R_{L\ eff}$ and the actual load resistance R_L. By varying the duty cycle of the PWM signal supplied to the gate of the MOSFET, the effective resistance of the load can be changed, so that it matches R_{TEG}.

$$R_{L\,eff} = \left(\frac{1 - D}{D}\right)^2 R_L \tag{13}$$

A circuit diagram of the SEPIC used is provided in Figure 4. The SEPC circuit was designed to operate at 10 kHz, where the relatively low frequency kept switching losses to a minimum; however this also meant that large passive components were needed to ensure the desired ripple current and voltage levels were not excessive. The 220 µH inductors and the 3900 µF capacitors gave the desired input and output voltage levels, while the 100 µF radial electrolytic capacitor was needed to handle the high ripple current at the isolation point. Table 4 details the components used in the construction of the SEPIC circuit. A photo of the SEPIC circuit is given in Figure 5.

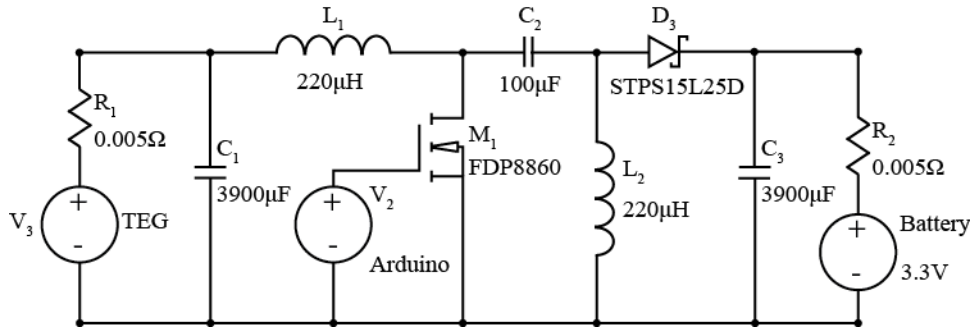

Figure 4: SEPIC DC-DC converter

Table 4: SEPIC List of Components

Part	Manufacturer	Manufacturer Part Number
3900µF electrolytic capacitor	Panasonic	EEUFR1C392L
100µF electrolytic capacitor	Sanyo	20SH100M
220µH Inductor	Murata Power Solutions	1422455C
N MOSFET	Fairchild Semiconductor	FDP8860
Schottky Diode	STMicroelectronics	STPS15L25D
0.005Ω resistor	Welwyn	OAR5-R005FI
Arduino Uno	Arduino	A000046

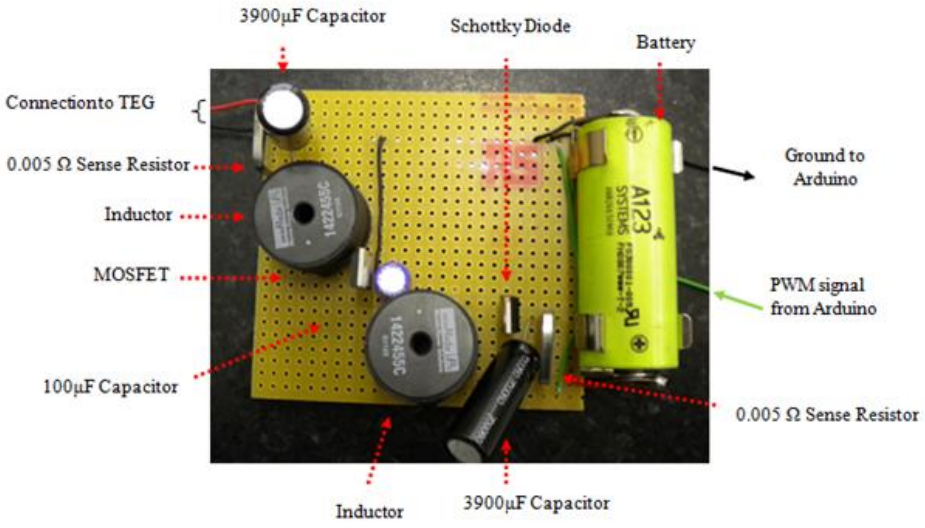

Figure 5: Photograph of the SEPIC circuit

In a SEPIC circuit, the input and output voltages are isolated by the capacitor C2 shown in Figure 4. Therefore if no voltage is applied to the gate of the MOSFET (duty cycle = 0), no current flows to the battery. This means it is possible to measure the open circuit voltage of the TEG for maximum power point tracking (MPPT). Two MPPT algorithms were coded with the SEPIC using an Arduino microcontroller. The purpose of the algorithms was to increase or decrease the duty cycle of the PWM signal supplied to the gate of the MOSFET until maximum power was supplied to the battery.

5.1 Open Circuit Voltage Method

As thermoelectric modules have linear current-voltage characteristics, the maximum power point voltage is equivalent to half the corresponding open circuit voltage of the TEG. The open circuit voltage method involves recording the open circuit voltage of the TEG and then varying the duty cycle of the PWM signal until the loaded voltage is half the open circuit voltage.

5.2 Combination Method

The second algorithm had two components. The first component used the characteristic equation of a SEPIC (as given by Equation 12) to set an initial duty cycle. At the maximum power point, the voltage across the TEG is equal to half the open circuit voltage (V_{OC}).

$$V_{in} = \frac{V_{oc}}{2} \tag{14}$$

If the output voltage is equal to the battery voltage, it follows that

$$D = \frac{V_{battery}}{\frac{V_{oc}}{2} + V_{battery}} \tag{15}$$

The Perturb and Observe method was then employed which involved measuring the current delivered to the battery with a current sense resistor. The duty cycle was increased and the current was measured again. If the current flowing into the battery increased with increasing duty cycle, the duty cycle was further increased. However if the current decreased with increasing duty cycle, the duty cycle was decreased.

6. Experimental set-up

To investigate in detail the behaviour of the TEGs under different operating conditions an experimental rig was constructed as shown in Figure 6. The rig was based on the design reported by Sandoz-Rosadoi and Stevens [4] and consists of a lower plate which is cooled by a water flow loop. The TEG sits on this surface. The upper surface is heated by cartridge heaters controlled by a variable power supply. The upper surface is lowered by a crank which enables the user to set the applied force on the TEG. The force applied to the TEG was measured with a load cell.

Copper plates were inserted between the TEG under test and the hot and cold surfaces of the apparatus and a thin layer of heat sink compound was applied between the TEG and the copper plates to reduce thermal contact resistance. Holes of 1 mm diameter were drilled into the copper plates and calibrated K-type thermocouples with an accuracy of +/- 1°C were inserted to measure the approximate hot and cold side temperature of the TEG. The cooling plate was positioned directly below the heating block and the crank was wound down until a pressure of 0.75 N/mm^2 was applied to the TEG. The temperature difference across the TEG was adjusted by varying the power to the cartridge heaters. Further details of the experimental rig can be found in O'Shaughnessy et al. [2].

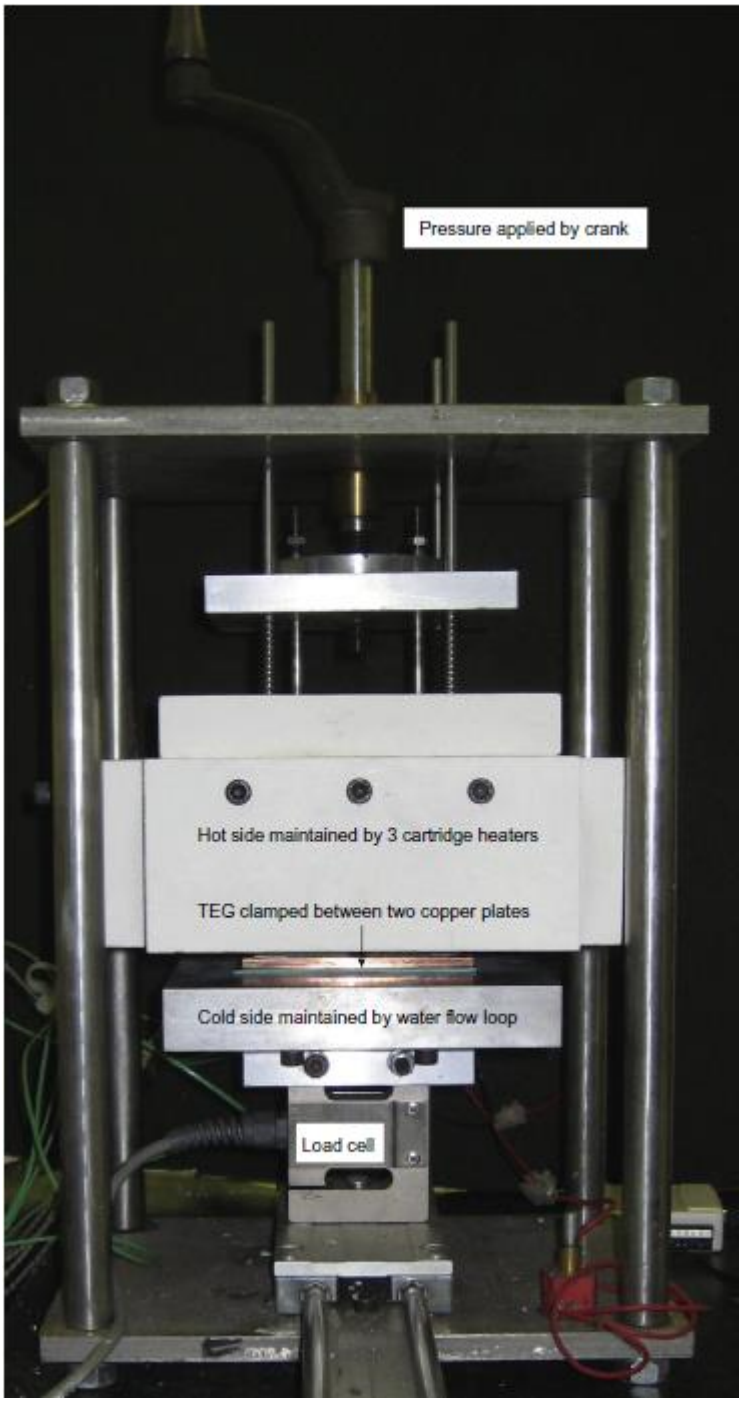

Figure 6: TEG testing apparatus

7. Experimental method and results

7.1 TEG characterisation

For a range of temperature differentials across the TEG (100 °C, 120 °C, 150 °C, 190 °C and 200 °C) the open circuit voltage of the TEG was measured using a digital multimeter. An electrical load was then attached to the TEG. Constantan wire was chosen as the load as it was capable of handling high currents and its resistivity remained relatively constant with varying temperature. The length of constantan wire, and thus the load resistance, was varied throughout the experiment. The voltage across the TEG was measured for a range of load resistances. The current was measured using a digital multimeter.

The results demonstrated the importance of load matching. Figure 7 shows the power produced by the TEG versus the load resistance applied. At ΔT_{TEG} ~100 °C, a maximum power of 2.18W was generated from the TEG when a 2.95 Ω resistance was connected in series with it. This implied the internal resistance of the TEG was 2.95 Ω at ΔT_{TEG} ~100 °C. The power generated by the TEG significantly decreased the further the load resistance moved away from the internal

resistance of the TEG. Importantly, the power-resistance curve is much steeper for load resistances less than the critical value. There was a small change in the internal resistance of the TEG with temperature. At ΔT_{TEG} ~200 °C, the internal resistance of the TEG increased to 3.17 Ω which is a 7% increase. On the other hand, the peak power increased to 5.3 W at ΔT_{TEG} ~200 °C, representing a 1.4-fold increase. The internal resistance of TEG at different temperature gradients is given in Table 5.

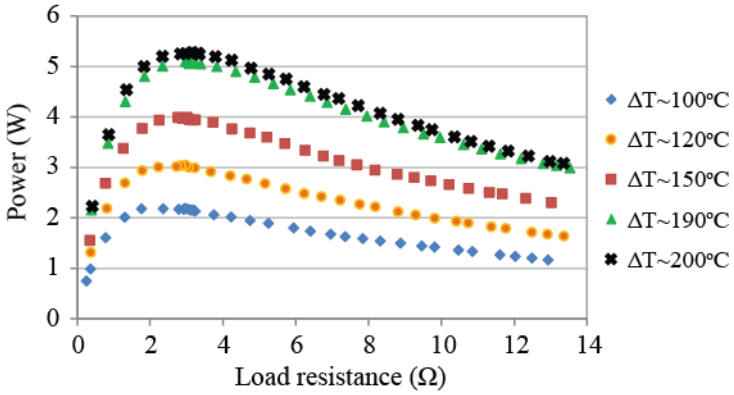

Figure 7: TEG output power versus load resistance

Table 5: Internal resistance of TEG1-12610-5.1

ΔT_{TEG} [°C]	Internal Resistance as specified by Manufacturer [Ω]	Tested Internal Resistance, [Ω]
100	2.2	2.95
120	2.6	2.98
150	3	3.02
190	3.2	3.02
200	3.3	3.17

Figure 8 illustrates the linear relationship between the voltage across the TEG and the current flowing through it. For a given ΔT_{TEG}, the intercept with the horizontal axis represents the open circuit voltage (i.e. zero current). Considering Figure 8 and Figure 9 it can be seen that maximum power was obtained from the TEG when the loaded voltage was equal to half the open circuit voltage as is expected.

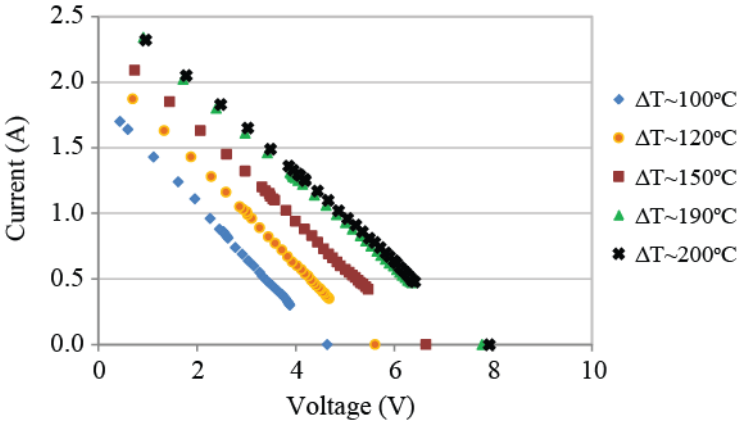

Figure 8: TEG voltage versus current

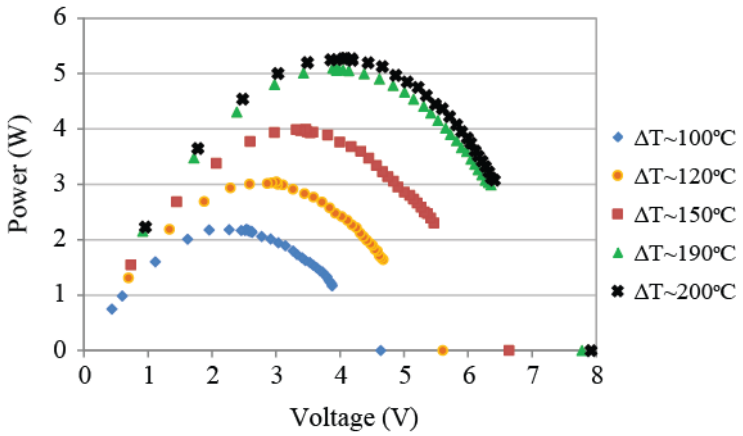

Figure 9: TEG voltage versus output power

When a load was applied to the TEG and current flowed through the circuit, the Peltier effect was observed whereby the temperature of the hot side decreased and the temperature of the cold side increased. Hence the Peltier effect decreased the temperature gradient across the TEG, reducing the power generated by the Seebeck effect. The temperature gradient across the TEG decreased by 8% when a 1.91 Amp current flowed through the circuit as shown in Figure 10. At high currents the Peltier effect was particularly prevalent.

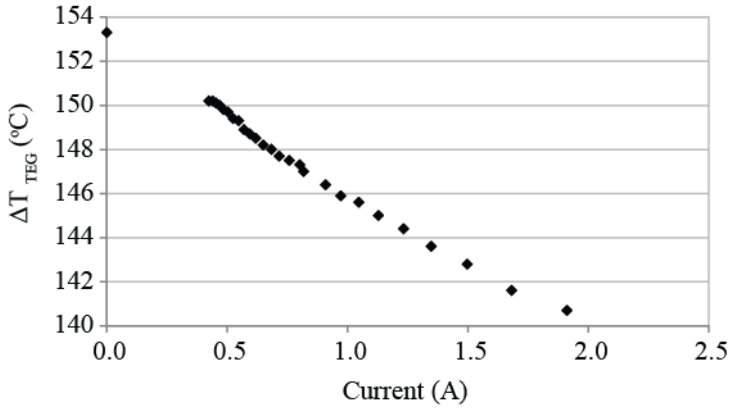

Figure 10: Peltier effect on TEG temperature differential

7.2 Direct charging the battery

The next set of experiments involved directly connecting the battery to the TEG (as in **Error! Reference source not found.**), with R_L representing the battery load. Before each experiment, the battery was discharged by connecting 3 Rolson white LED lamps in parallel to the battery. The battery was disconnected when the LEDs turned off, which occurred when the battery was discharged to 2.5 V. This ensured the same starting conditions for each test. The TEG was connected to the battery until the battery voltage reached 3.8V, the maximum recommended charge voltage specified by the manufacturer. The TEG was then disconnected. The experiment was repeated for a range of temperature gradients across the TEG (100 °C, 120 °C, 150 °C, 190 °C and 200 °C). The current was measured using a 0.005 Ω current sense resistor.

The results demonstrated the flat voltage characteristics of Lithium Iron Phosphate batteries during charging. When the TEG was directly connected to the battery, the voltage across the TEG was equal to the battery voltage, regardless of the temperature gradient across the TEG as demonstrated in Figure 11.

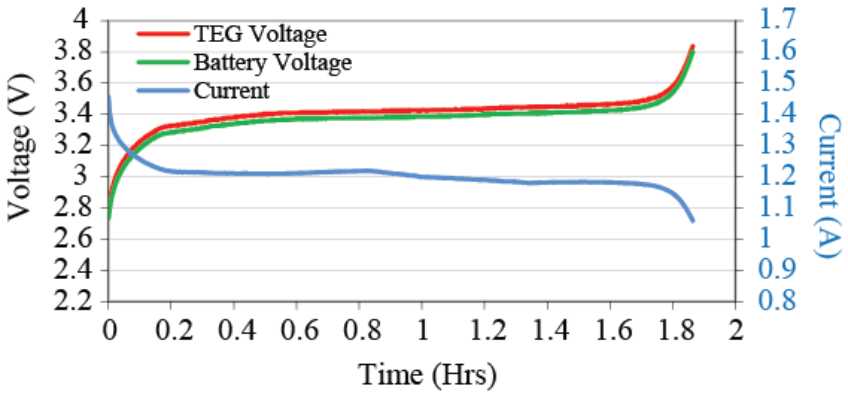

Figure 11: Direct battery charging with ΔTTEG ~ 150 ^{0}C

For 80% of the charge cycle, the battery voltage remained between 3.3 and 3.4 V. The battery voltage then increased exponentially. The TEG was disconnected as soon as the battery voltage reached 3.8V, however the battery was not fully charged at this point. The current flowing into the battery also remained relatively constant during 80% of the charge cycle and was dependent on the temperature gradient across the TEG as demonstrated in Figure 12. This indicates that the effective impedance of the battery remains constant over the majority of its charge cycle.

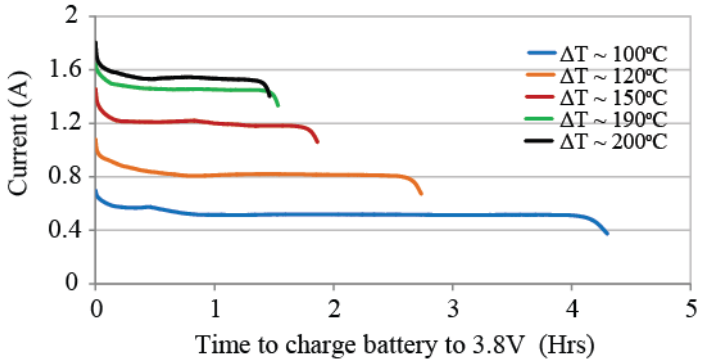

Figure 12: Current supplied to the battery by direct charging for a range of ΔTTEG

Likewise the power supplied to the battery remained relatively constant during 80% of the charge cycle and was dependent on the temperature gradient across the TEG as demonstrated in **Error! Reference source not found.**.

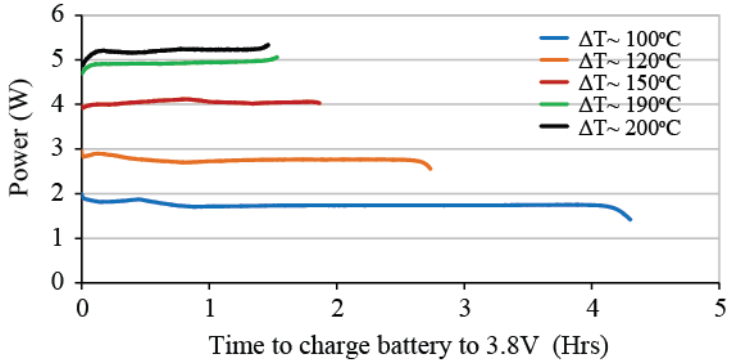

Figure 13: Power supplied to the battery by direct charging for a range of ΔTTEG

The results indicate that when the battery was directly connected to the TEG, the matched load condition occurred at ΔT_{TEG} ~150 °C, where, as shown in Figure 14, the effective resistance of the battery was between 2.75 Ω – 3 Ω for the majority of the charging cycle. This was close to the internal resistance of the TEG at ΔT_{TEG} ~150 °C as given in Table 5.

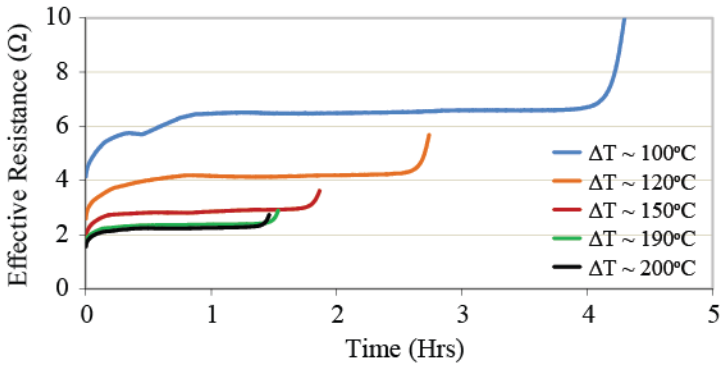

Figure 14: Effective resistance of the battery for a range of ΔTTEG

It was found that at temperature gradients above 120 °C, the effective resistance of the battery was close to the internal resistance of the TEG. However at temperature gradients below 120 °C, there was a large mismatch between the internal resistance of the TEG and the effective resistance of the battery as illustrated by comparing results in Figure 14 and Table 5. This resulted in a reduction in the power delivered to the battery. At 120 °C, Figure 7 previously showed that the maximum power available from the TEG was 3 W while Figure 13 illustrates that when the battery was directly connected to the TEG, only 2.75 W was delivered to the battery. This suggested that maximum power point tracking would be beneficial for temperature gradients below 120 °C.

7.3 SEPIC DC-DC converter testing

A SEPIC DC-DC converter was connected between the TEG source and lithium iron phosphate battery. Initially, the duty cycle was controlled manually so that the SEPIC could be characterised over its full operating range. A 10 kHz PWM signal was supplied by an Arduino microcontroller which was externally powered. The duty cycle of the PWM signal was incrementally increased from 0-100% and the power into and out of the DC-DC converter was measured using digital multimeters. The experiment was repeated for a range of temperature gradients across the TEG.

The effective resistance of the battery load (seen at the output of the SEPIC) decreased with increasing duty cycle as shown in Figure 15. This is as predicted by Equation 13 and as expected, maximum power was delivered to the battery when the effective resistance of the load was equal to the internal resistance of the TEG; i.e. 2.6 Ω for ΔT_{TEG} ~80 °C.

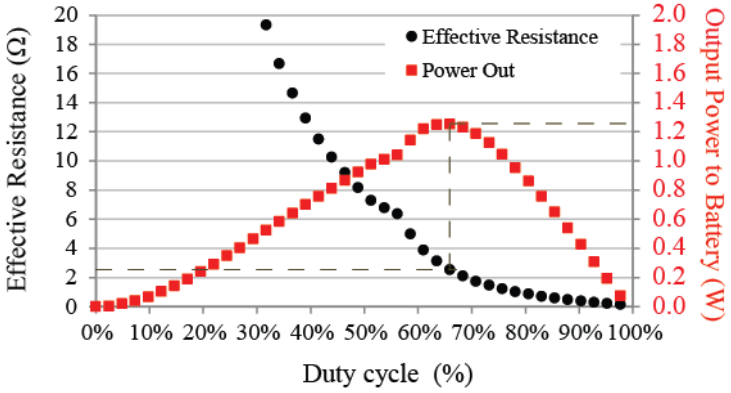

Figure 15: Effective resistance and output power at ΔTTEG ~80 °C with varying duty cycle

At the matched load point, the efficiency of SEPIC was 85% as shown in Figure 16.

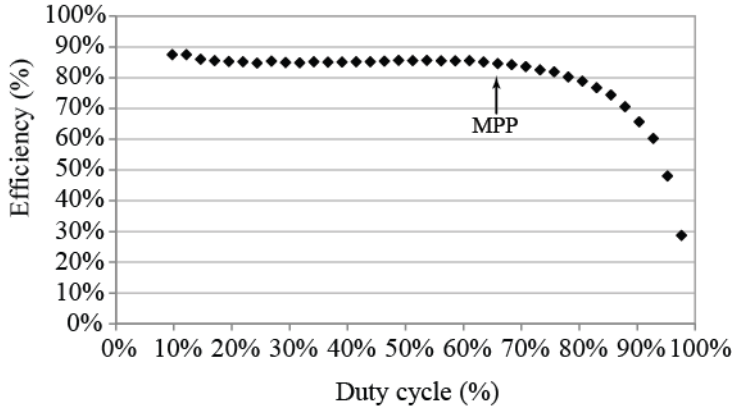

Figure 16: Efficiency of 10 kHz SEPIC at ΔTTEG ~80 °C

The power delivered to the battery depended on the temperature gradient across the TEG and the duty cycle of the PWM signal as shown below in Figure 17.

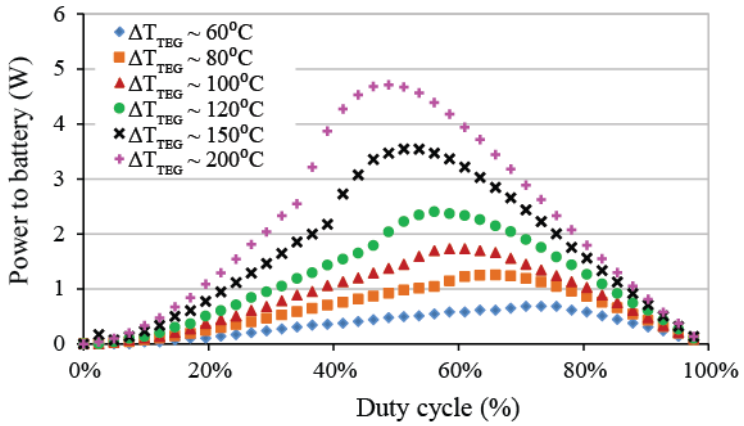

Figure 17: Power delivered to the battery with SEPIC inserted between the TEG and the battery

Plotting the maximum values of power from Figure 17 for each test temperature gradient as shown in Figure 18, it was found that above ΔT_{TEG} ~100 °C, more power was delivered to the battery by direct charging rather than by employing a DC-DC converter. Although there was a large mismatch between the internal resistance of the TEG (2.95 Ω) and the effective resistance of the battery (6.5 Ω) at ΔT_{TEG} ~100 °C, it was still comparable to direct charging or using a DC-DC converter. While the DC-DC converter did reduce the impedance mismatch, it also increased losses in the circuit. This highlights that the insertion of a DC-DC converter is not appropriate when the effective resistance of the load is within a certain range of the internal resistance of the TEG.

The temperature range for which a DC-DC converter provides improved performance may be determined by comparing the shortfall in power from the maximum power available (due to impedance mismatch) with DC-DC converter losses. The DC-DC converter should be included if its losses are significantly lower than the maximum power point shortfall. For example, at ΔT_{TEG} ~100 °C, the results of Figure 9 show that a maximum power of 2.18 W is available, but only 1.74 W is achieved if the TEG operating voltage is fixed at 3.3 V by direct connection of the battery load (see Figure 13). In this case, a DC-DC converter would provide improved performance if it had losses less than ~ 0.44 W. As shown in Figure 16, the given SEPIC converter has an efficiency of ~85% which corresponds to losses of ~ 0.33 W for an input power of 2.18 W. Therefore the inclusion of a converter would provide a 0.11 W (~ 5%) improvement in output power and may be taken as a cut-off point.

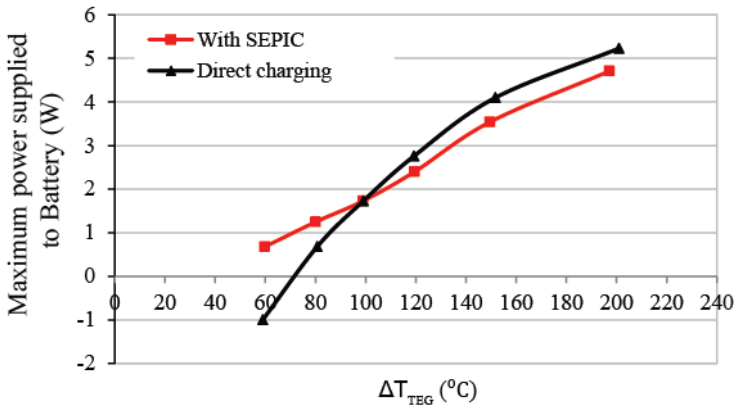

Figure 18: Comparison of the maximum power delivered to the battery

In addition to improved output power, Figure 18 highlights another advantage of inserting a DC-DC converter when the TEG voltage is below the battery voltage. At ΔT_{TEG} ~60 °C the TEG acted as a load and discharged the battery. By inserting a DC-DC converter it was still possible to charge the battery even though the TEG voltage was lower than the battery voltage.

8. Maximum Power Point Tracking Algorithms

In order to illustrate the effectiveness of maximum power point tracking, the two algorithms considered were tested on the 10 kHz SEPIC circuit with an 80 °C temperature gradient maintained across the TEG; i.e. where the mismatch in source and load impedance is significant. Once the MPPT reached its maximum power point, the duty cycle was held constant for a period of time. This was repeated thirty three times to ensure repeatability of results. The maximum power delivered to the battery using the Open Circuit Voltage MPPT algorithm was 1.24 W and the minimum power delivered was 1.17 W. The results are illustrated in Figure 19 below:

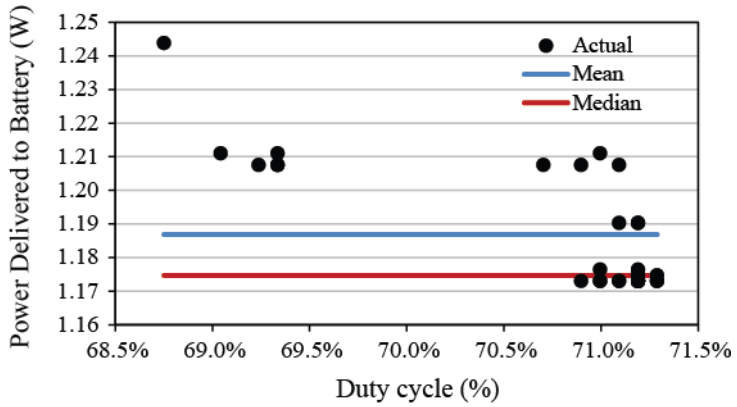

Figure 19: Power delivered to the battery using the Open Circuit Voltage MPPT algorithm

The maximum power delivered to the battery using the Combination MPPT algorithm was 1.22 W and the minimum power delivered was 1.07 W. The results are shown in Figure 20.

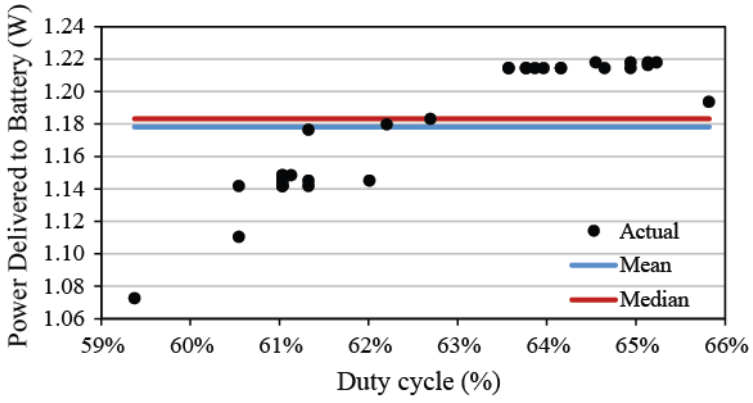

Figure 20: Power delivered to the battery using the Combination MPPT algorithm

There was larger variability in the duty cycle using the Combination MPPT due to the Perturb and Observe element of the technique. Depending on the point in the switching cycle, the current may increase or decrease, irrespective of a change in duty cycle. This slightly distorted the Perturb and Observe effectiveness as a MPPT technique.

Nonetheless, as shown in Figure 21, both algorithms located close to the maximum power point found in Figure 17 when the duty cycle was varied manually. In that case, maximum power delivered to the battery was 1.26 W, with a duty ratio of 64%.

The results demonstrated that the Open Circuit Voltage MPPT algorithm on average delivered slightly more power to the battery (1.19 W) than the Combination MPPT algorithm (1.18 W). However both algorithms were close to the maximum power point (1.26 W) and considerably better than direct charging (0.68 W).

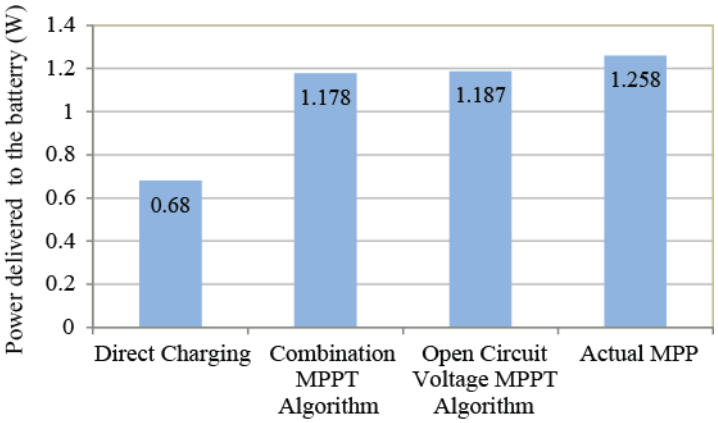

Figure 21: Power to the battery with ΔTTEG ≈ 80 °C

9. Discussion

The results illustrated that for temperature gradients above 100 °C across the TEG, more power was delivered to the battery by direct charging. For temperature gradients below 100 °C, more power was delivered to the battery by employing a DC-DC converter. It was found that either the Open Circuit Voltage or the Combination algorithm closely matched the maximum power point.

Therefore, for situations where temperature gradients are above 100 °C it is not necessary to employ a DC-DC converter. This is because the battery was carefully selected so that the nominal voltage of the battery was close to the loaded voltage of the thermoelectric module in the expected operating range. Thus, a much simplified circuit is proposed and is discussed below.

In order to protect the battery from over-charge, a simple form of charge protection was designed to limit the battery voltage as shown in Figure 22. A Schottky diode was placed in front of the battery to prevent it discharging at low temperature gradients across the TEG and a 3.9 V Zener diode was placed in parallel with the battery, to limit the battery voltage. The Zener diode had to be able to take the full output power of the TEG, therefore a 5 W Zener diode was selected.

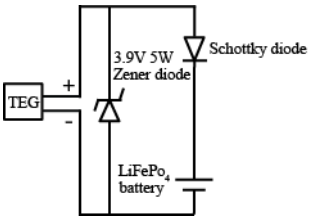

Figure 22: Charge Protection Circuitry

It was found that when the Zener diode was fully enabled (3.9 V), the current flowing into the battery dropped to zero, fully protecting the battery from overcharge. The major disadvantage of using the Zener diode was that even below the Zener voltage, a significant amount of leakage current flowed through the Zener diode (~0.14 A) as demonstrated in Figure 23. The specifications of the Zener quoted that the reverse leakage current would be 50 µA at 1 V, but the reverse leakage current was much greater at the battery's nominal voltage (3.3 V).

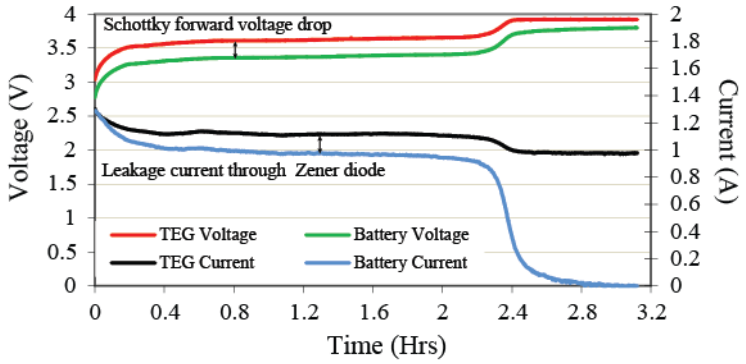

Figure 23: Charge Protection Circuit in place, ΔTTEG ~150^{0}C

In Figure 23, the difference between the TEG current and the battery current was equal to the current flowing through the Zener diode. The reverse leakage current did not vary with charging current. At ΔT_{TEG} ~ 100 °C, when the TEG current was only ~ 0.43 A, the proportion of current leaking through the Zener diode was particularly significant (~30%). However at ΔT_{TEG} ~200 °C, the proportion was less significant (~10%).

As shown in Figure 24, at ΔT_{TEG} ~100 °C, it took 3.44 hours for the battery voltage to increase from 3.3 V to 3.6 V during direct charging. This increased to 6.5 hours with the Zener and Schottky diode in place. The effective resistance of the load increased from 6.5 Ω (direct charging) to 8.4 Ω (with charge protection circuit). Thus a larger mismatch existed between the internal resistance of the TEG (2.95 Ω) and the effective resistance of the load, resulting in reduced power and increased charge time.

At ΔT_{TEG} ~200 °C, it took 1.24 hours for the battery voltage to increase from 3.3V to 3.6V during direct charging and 1.52 hours with the Zener diode circuit. In this case, the effective resistance of the load with the charge protection circuit (2.5 Ω) was closer to the internal resistance of the TEG (3.17 Ω) than during direct charging (2.23 Ω). Thus at high temperature gradients across TEG, the charge protection circuit provided better load matching.

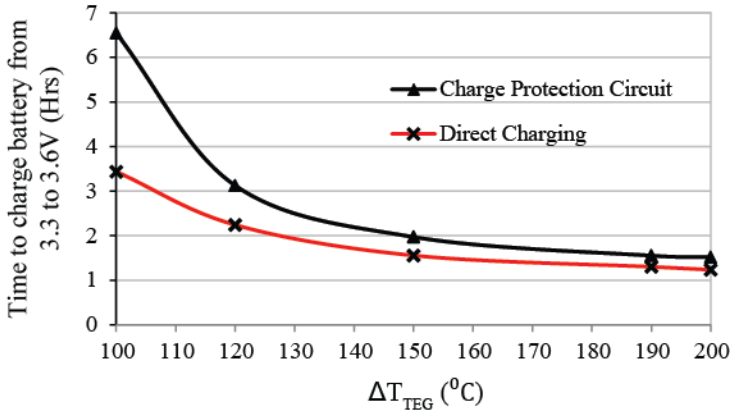

Figure 24: Time to charge the battery from 3.3V to 3.6V for varying ΔTTEG

Additional features were added to the simple charge protection circuit to increase its safety characteristics as shown in Figure 25.

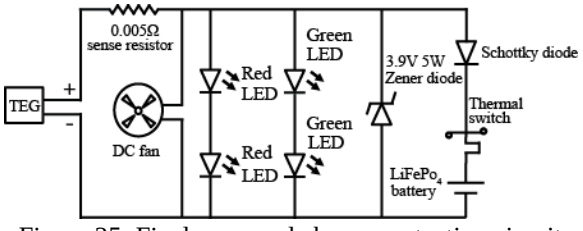

Figure 25: Final proposed charge protection circuit

A bimetallic thermal switch was connected in series with the battery. The battery was positioned above the thermal switch so that if the battery temperature exceeded 60 °C, the bimetallic switch would open, disconnecting the battery from the power source.

Green and red LEDs were placed in parallel with the TEG and battery. The purpose of the green LEDs was to indicate when the battery was fully charged. The purpose of the red LEDs was to indicate that the TEG was connected. The proposed circuit protected the battery from over-charge. At high temperature gradients across the TEG (close to 200 °C), the circuit helped to reduce the mismatch between the internal resistance of the TEG and the effective resistance of the load.

10. Conclusion

In-depth analysis was carried out to deliver maximum power from a single thermoelectric module to a rechargeable lithium iron phosphate battery. It was discovered that at temperature gradients below ΔT_{TEG} = 100 °C, it was beneficial to employ a SEPIC DC-DC converter. However above ΔT_{TEG} = 100 °C more power was delivered to the battery by direct charging.

For temperature gradients of 150 °C to 200 °C, the charge protection circuit provides a simple, inexpensive and robust charging solution. This circuit has been used recently by the current authors for a development project whereby a TEG generator system was designed to generate electricity from biomass cookstoves in the developing world [2]. The circuit has proven to work as designed for extended periods of time and the end users charged mobile phones and LED lanterns.

Nomenclature

Symbol	Description	Unit
A	cross-sectional area of a single thermo-element	m^2
I	current	A
I_m	Current at matched load	A
L	Length of thermo-element	m
L_c	Contact layer thickness	m
N	Number of thermo-elements	-
P_{elec}	Electrical power	W
Q_H	Heat delivered to TEG hot side	W
Q_C	Heat dissipated from TEG cold side	W
R_L	Load resistance	Ω
R_{TEG}	TEG internal resistance	Ω
T_h	Module hot side temperature	K
T_c	Module cold side temperature	K
ΔT_{TEG}	Module temperature difference	K
V	Voltage	V
V_m	Voltage at matched load	V
V_{oc}	Open circuit voltage	V
Z	Figure of merit	1/K
α	Seebeck coefficient	V/K
α_{eff}	Seebeck coefficient	V/K
$\alpha_{p,n}$	Seebeck coefficient of p/n element	V/K
λ	Thermal conductivity	W/mK
λ_c	Contact thermal conductivity	W/mK
$\lambda_{p,n}$	Thermal conductivity of p/n element	W/mK
ρ	Electrical resistivity	Ωm
ρ_c	Electrical contact resistivity	Ωm

TEG	Thermoelectric Generator	-
TEM	Thermoelectric Module	-
PWM	Pulse Width Modulated	-
MPPT	Maximum Power Point Tracking	-
MOSFET	Metal Oxide Semiconductor Field Effect Transistor	-
SEPIC	Single Ended Primary Inductor Converter	-

Acknowledgments

The authors would like to gratefully acknowledge Irish Aid, Electric Aid, Cara Malawi, The Irish Research Council for Science & Engineering Technology (IRCSET), and Intel Corporation for their support and contribution to this research, and also Concern Universal for their continued assistance in the field.

References

[1] Riffat SB, Ma X. Thermoelectrics: a review of present and potential applications. Applied Thermal Engineering. 2003;23:913-35.

[2] O'Shaughnessy SM, Deasy MJ, Kinsella CE, Doyle JV, Robinson AJ. Small scale electricity generation from a portable biomass cookstove: Prototype design and preliminary results. Applied Energy. 2012.

[3] Lesage FJ, Pagé-Potvin N. Experimental analysis of peak power output of a thermoelectric liquid-to-liquid generator under an increasing electrical load resistance. Energy Conversion and Management. 2013;66:98-105.

[4] Sandoz-Rosado E, Stevens R. Experimental Characterization of Thermoelectric Modules and Comparison with Theoretical Models for Power Generation. Journal of Elec Materi. 2009;38:1239-44.

[5] Rodríguez A, Vián JG, Astrain D, Martínez A. Study of thermoelectric systems applied to electric power generation. Energy Conversion and Management. 2009;50:1236-43.

[6] Hodes M. On one-dimensional analysis of thermoelectric modules (TEMs). IEEE Transactions on Components and Packaging Technologies. 2005;28:218-29.

[7] Hsu CT, Huang GY, Chu HS, Yu B, Yao DJ. An effective Seebeck coefficient obtained by experimental results of a thermoelectric generator module. Applied Energy. 2011.

[8] Eakburanawat J, Boonyaroonate I. Development of a thermoelectric battery-charger with microcontroller-based maximum power point tracking technique. Applied Energy. 2006;83:687-704.

[9] Nagayoshi H, Kajikawa T. "Mismatch Power Loss Reduction on Thermoelectric Generator Systems Using Maximum Power Point Trackers". Proceedings of the 25th International Conference on Thermoelectrics,2006. p. 210-3.

[10] Nagayoshi H, Tokumisu K, Kajikawa T. "Evaluation of multi MPPT thermoelectric generator system". Proceedings of the 26th International Conference on Thermoelectrics,2007. p. 318-21.

[11] Lihua C, Dong C, Yi H, Peng FZ. "Modeling and power conditioning for thermoelectric generation". Power Electronics Specialists Conference, 20082008. p. 1098-103.

[12] Vieira JAB, Mota AM. "Thermoelectric generator using water gas heater energy for battery charging". 18th IEEE International Conference on Control Applications2009. p. 1477-82.

[13] Rowe DM. Thermoelectric power generation. Proceedings of the Institution of Electrical Engineers. 1978;125:1113-36.

[14] Rowe DM. Thermoelectric generators as alternative sources of low power. Renewable energy. 1994;5:1470-8.

[15] Rowe DM, Min G. Evaluation of thermoelectric modules for power generation. Journal of Power Sources. 1998;73:193-8.

[16] Brodd RJ. Batteries for Sustainability: Selected Entries from the Encyclopedia of Sustainability Science and Technology: Springer; 2012.